energy&fuels

pubs.acs.org/EF

Article

Polymer-Enhanced Active Layer Crystallization in Low-Temperature Carbon-Based Perovskite Solar Cells

Shih-Han Huang, Yu-Hsiang Chen, Hou-Chin Cha, Damian Glowienka, Ming-Chung Wu,* and Yu-Ching Huang*

Cite This: https://doi.org/10.1021/acs.energyfuels.4c03898

Read Online

ACCESS | Metrics & More | Article Recommendations | Supporting Information

ABSTRACT: High-efficiency perovskite solar cells (PSCs) are emerging as a promising next-generation, low-cost, photovoltaic technology. A key advantage of PSCs is their compatibility with diverse manufacturing techniques, enabling the pursuit of low-cost, stable PSCs. Carbon electrodes, known for their scalability, chemical inertness, and ease of processing through screen printing, have recently seen the development of low-temperature carbon electrodes with high conductivity for use in PSCs. However, optimizing low-temperature carbon-based PSCs (LTC-PSCs), particularly improving the interface between the perovskite and carbon electrodes, remains a significant challenge. In this study, poly(3-hexylthiophene-2,5-diyl) (P3HT) was employed as an additive and a hole-transporting layer (HTL) in LTC-PSCs with low-temperature screen-printing carbon electrodes. The incorporation of P3HT in antisolvent improved the perovskite/carbon interface, reducing the defect density of the perovskite layer. This resulted in a significant average power conversion efficiency (PCE) improvement of 11%. The LTC-PSCs achieved a PCE of 10.90% and demonstrated exceptional stability, retaining 90% of initial PCE after 1200 h under ambient air. This research highlights the potential of LTC-PSCs as low-cost strategies for the commercialization of PSCs.

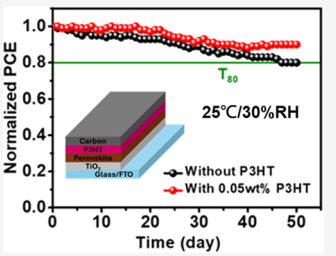

1. INTRODUCTION

Solution-processable perovskite solar cells (PSCs) with the highest growth in power conversion efficiency (PCE) have emerged as a potential next-generation low-cost photovoltaic technology.[1−3] However, many challenges must be overcome to promote commercialization of this technology to commercialization. For instance, the lifetime issue of the device still limits commercialization progress, which is attributed to the decomposition of the perovskite layer. This degradation is often induced by the diffusion of metal atoms from the top electrode and dopant ions from charge-transporting materials (CTM) like lithium in Spiro-OMeTAD.[4−8] Commonly, PSCs have utilized high-cost metal electrodes like gold or silver, necessitating deposition under ultravacuum conditions, thereby inflating manufacturing costs. C-PSCs have emerged as a viable solution to enhance the stability and reduce manufacturing expenses. Carbon electrodes offer chemical inertness and compatibility with scalable deposition techniques like screen-printing, presenting promising potential for mass production.[9−12]

The initial configuration of carbon electrode-integrated PSCs involved a fully printable mesoscopic layer (TiO_2/ZrO_2/carbon), requiring high-temperature curing at approximately 500 °C. Following the assembly of the triple mesoscopic structure, the perovskite solution is applied to permeate through the carbon electrode, facilitating the formation of the perovskite layer within the structure.[13−15] To date, high-temperature carbon-based perovskite solar cells (HTC-PSCs) have achieved PCEs exceeding 17%,[16,17] with encapsulated devices maintaining 90% of their initial PCE after 1000 h of aging at 85 °C in ambient condition.[16] Although HTC-PSCs have shown promising results, their performance still lags behind that of PSCs using metal electrodes. The high-temperature process of HTC-PSCs poses several limitations, including restricted choices of CTMs, poor perovskite pore-filling, and fabrication on only rigid substrates. To address these limitations, developing low-temperature carbon electrodes offers several advantages over HTC-PSCs.[18,19] Low-temperature carbon electrodes enable direct deposition atop the perovskite layer, mitigating pore-filling challenges and enhancing manufacturing compatibility with conventional PSC technologies.

Furthermore, optimization efforts for low-temperature carbon-based PSCs (LTC-PSCs) have mainly focused on improving the interface between the perovskite and carbon electrodes. Effective interface contact requires high-quality perovskite films and efficient charge extraction to the carbon electrode. Two critical factors influencing the modest PCE of C-PSCs include the energy level alignment between the

Received: August 12, 2024
Revised: December 18, 2024
Accepted: December 19, 2024

perovskite layer and carbon electrodes and the defect density within the perovskite film. In the absence of HTLs in n-i-p C-PSCs, direct contact between the perovskite layer and carbon electrode leads to substantial energy offsets, hindering hole extraction and resulting in significant charge recombination losses.[20,21] Second, the quality of the perovskite film is crucial for achieving good interface contact and is determined by the defects within the film in C-PSCs. In the conventional process, antisolvent dripping is a facile method to prepare uniform perovskite films, but the rapid precipitation of perovskite crystals with small grains easily forms boundary defects. Post-treatment strategies are commonly employed to modify defect formation.[22−27] Additive engineering has effectively controlled the defect formation. In previous studies, poly(ethylene glycol) (PEG) was introduced into the perovskite precursor solution, improving the quality of perovskite films for different coating techniques.[28−30] Bi et al. first incorporated poly(methyl methacrylate) (PMMA) into the antisolvent for perovskite fabrication, with the polymer serving as a nucleation site to facilitate perovskite crystal growth.[31] Qin et al. further chose the donor polymer poly[(2,6-(4,8-bis(5-(2-ethylhexyl) thiophen-2-yl)-benzo[1,2-b:4,5-b′]dithiophene))-*alt*-(5,5-(1′,3′-di-2-thienyl-5′,7′-bis(2-ethylhexyl)benzo[1′,2′-*c*:4′,5′-*c*′]-dithiophene-4,8-dione)]) (PBDB-T) to add into the antisolvent.[32] The results demonstrate that PBDB-T serves as a heterogeneous nucleation site and passivates the trap state of uncoordinated Pb in the perovskite films. It shows the effectiveness of the polymer additive for defect passivation, which can be an effective path to solve the performance loss in LTC-PSCs.

In this work, a comprehensive optimization of LTC-PSC is developed. First, the low-temperature carbon electrode is fabricated using the screen-printing method. Considering the interface issue, P3HT exhibits better contact with low-temperature carbon electrodes than other HTLs. Subsequently, P3HT is introduced into the antisolvent to control the quality of the perovskite film. This results in an improvement in the interface between the perovskite and HTL, and a reduction in the defect density of the perovskite film, leading to an average PCE improvement of 11% with polymer additives in LTC-PSCs. The highest PCE of the LTC-PSCs can reach 10.90%. Unencapsulated LTC-PSCs retain 90% of the initial PCE after 1200 h in ambient air for the stability test. LTC-PSCs demonstrate excellent stability and offer a low-cost technique to facilitate the commercialization of perovskite solar cells.

2. MATERIALS AND METHODS

2.1. Preparation of Precursor Solution. For the preparation of the TiO_2 precursor solution, the first solution of 40 g of titanium isopropoxide ($Ti(OCH(CH_3)_2)_4$, TTIP, 99.99%, ACROS) was added into 20 mL of isopropanol (IPA, 99.5+% extra pure, ACROS). An acetic acid solution containing 30 mL of acetic acid (99.5%, ACROS) and 170 mL of deionized water was added dropwise into the TTIP solution in an ice bath with continuous stirring. After 12 h of stirring, the solution was kept at 90 °C for 10 h to react. The 1.8 M perovskite solution was prepared with a mixed ratio (1:1) of lead iodide (PbI_2, 99.9985%, Alfa Aesar) and methylammonium iodide (CH_3NH_3 I, MAI, FrontMaterials), dissolved in a mixture solution of γ-butyrolactone (GBL, ≥99%, Sigma-Aldrich) and dimethyl sulfoxide (DMSO, 99.9%, ECHO) with a 1:1 volume ratio. For polymer additive, the P3HT (>95%, RIEKE) solutions were made at 0.01, 0.05, and 0.10 wt % concentrations in antisolvent. To achieve these concentrations, 0.1, 0.5, and 1 mg of P3HT were dissolved in 1 mL of chlorobenzene (CB, 99.8%, ACROS), respectively. The Spiro-OMeTAD solution consisted of 80 mg of 2,2′,7,7′-tetrakis[*N*,*N*-di(4-methoxyphenyl)amino]-9,9′-spirobifluorene (Spiro-OMeTAD, FrontMaterials) in 1 mL of CB. Then, 2.6 μL of lithium bis(trifluoromethanesulfonyl)imide solution (Li-TFSI, 98+, Alfa Aesar) (100 mg/mL in acetonitrile) was added, followed by 1.5 μL of 4-*tert*-butylpyridine (tBP, 98%, Sigma-Aldrich). Other HTL solutions, such as PM6 (>95%, 1-material), PCDTBT (>95%, 1-material), PBDB-T (>95%, 1-material), PTB7-TH (>95%, 1-material), and P3HT, were prepared using the same grams as Spiro-OMeTAD. Carbon paste (SC-1010, Advanced Electronic Materials, Inc.) was used as the commercial product without treatment.

2.2. Fabrication of Perovskite Solar Cells. 10 × 10 cm^2 FTO substrate (sheet resistance of 7 Ω/□, Ruilong) was cleaned by sequential sonication in detergent, acetone, and isopropanol. Then, the FTO substrate was ultraviolet (UV)-ozone cleaned for 30 min. The TiO_2 precursor solution was spray-coated on the FTO substrate at 450 °C for 30 min to form a dense TiO_2 layer.[33] The dilute mesoporous TiO_2 paste was screen-printed on a dense TiO_2 layer and calcined at 500 °C for 30 min. After the calcination of TiO_2, the substrate was cut to a 2.5 × 2.5 cm^2 size. The following steps were prepared in a glovebox. 50 μL of the perovskite precursor solution was spin-coated at 1000 rpm for 10 s and 4500 rpm for 20 s, respectively. After spinning at 4500 rpm for 17 s, 120 μL of antisolvent CB was dropped onto the substrate during spin-coating. Different concentrations of P3HT were dissolved in the antisolvent CB for antisolvent dripping. The as-prepared perovskite film was annealed at 100 °C for 20 min. For the HTL layer, 25 μL of HTL solution was spin-coated at 3000 rpm for 20 s. For the metal electrode, 120 nm of Ag electrode was thermally evaporated on the device with a shadow mask. Finally, the carbon electrode was screen-printed on the device with a shadow mask of 0.09 cm^2. The drying methods for the carbon electrode included heating and vacuum techniques, respectively. The heating method involved using a hot plate set to 80 °C for 30 min. The vacuum method involved storing the samples in a vacuum chamber at −0.1 MPa overnight.

2.3. Materials and Devices Characterization. Measurements were performed by using a voltage source meter (Keithley 2410) under an AM 1.5G solar simulator with 100 mW/cm^2 irradiation. Time-resolved PL (TRPL) measurements were performed by exciting samples with a 532 nm diode laser (LDH−P-C-405, PicoQuant). The TRPL was recorded by a system (UniDRON-plus, UniNano Tech). Transient photovoltage (TPV) decay, transient photocurrent (TPC) decay, and electrochemical impedance spectroscopy (EIS) analysis measurements of PSCs were recorded with Paios (Fluxim, electrical measurement all-in-one platform for solar cells). The surface morphology of the film was studied by scanning electron microscopy (SEM) (JSM-7610F, JEOL Ltd.) and atomic force microscopy (AFM) (Dimension-3100 Multimode, Digital Instruments). The external quantum efficiency (EQE) was measured by a system (QE-R, Enlitech).

3. RESULTS AND DISCUSSION

3.1. Optimization of Low-Temperature Carbon Electrode. The manufacturing of the carbon electrode was carried out using the screen-printing method, which is well established in dye-sensitized solar cells. The screen-printing process uses carbon paste, which can be classified into two types: high- and low-temperature carbon paste, depending on the binder formulation in the paste. The binder improves the carbon film's quality but hinders the carbon electrode's conductivity. High-temperature carbon paste requires high-temperature sintering to obtain high-quality carbon electrodes. For the low-temperature carbon paste, the quality of the carbon electrode is influenced by the amount of binder in the paste. Therefore, drying the low-temperature carbon electrode is critical. First, the carbon electrode was prepared using different drying methods, such as heating and vacuum drying. Figure S1 presents the morphology of the carbon electrodes by using

https://doi.org/10.1021/acs.energyfuels.4c03898
Energy Fuels XXXX, XXX, XXX−XXX

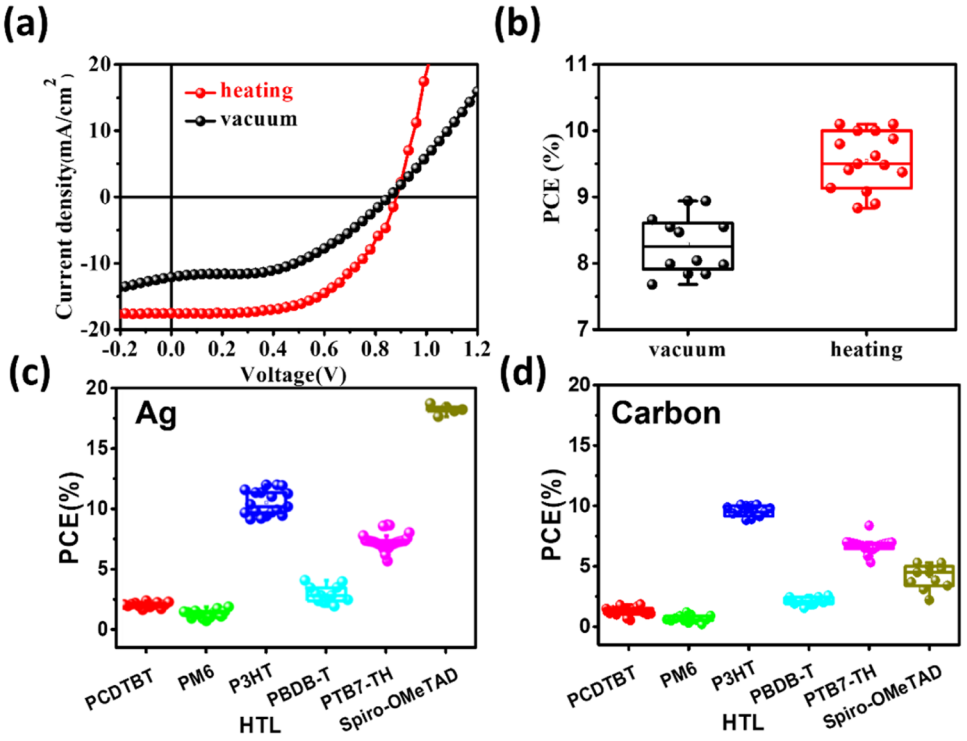

Figure 1. (a) $J-V$ curves and (b) PCE distribution of LTC-PSCs prepared using different drying processes for the carbon electrode. PCE distribution of PSCs was prepared using different HTLs with different electrodes: (c) Ag and (d) carbon electrodes.

Table 1. Device Performance of the Ag-PSCs and LTC-PSCs Prepared by Using Different HTLs

HTL/Ag	V_{oc} (V)	J_{sc} (mA/cm^2)	FF (%)	PCE$_{avg}$ (%)
PCDTBT	0.90 ± 0.02	8.85 ± 0.23	20.94 ± 2.16	1.67 ± 0.22
PM6	0.90 ± 0.03	4.18 ± 0.54	18.80 ± 1.71	0.69 ± 0.41
P3HT	0.91 ± 0.03	19.04 ± 1.04	55.13 ± 2.93	10.23 ± 1.04
PBDB-T	0.88 ± 0.04	11.86 ± 0.27	19.01 ± 3.71	2.06 ± 0.14
PTB7-TH	0.97 ± 0.01	18.15 ± 0.21	49.39 ± 1.02	8.14 ± 0.71
Spiro-OMeTAD	1.05 ± 0.02	23.01 ± 0.46	76.22 ± 1.21	17.75 ± 0.56
HTL/Carbon	V_{oc} (V)	J_{sc} (mA/cm^2)	FF (%)	PCE$_{avg}$ (%)
PCDTBT	0.90 ± 0.02	7.61 ± 0.23	21.07 ± 2.42	1.21 ± 0.45
PM6	0.90 ± 0.03	2.18 ± 0.37	19.12 ± 1.03	0.39 ± 0.33
P3HT	0.91 ± 0.03	19.04 ± 1.10	55.13 ± 1.84	9.54 ± 1.04
PBDB-T	0.88 ± 0.04	9.31 ± 0.42	19.01 ± 1.31	1.97 ± 0.58
PTB7-TH	0.91 ± 0.01	17.15 ± 0.21	45.01 ± 1.02	7.01 ± 2.35
Spiro-OMeTAD	0.97 ± 0.04	14.04 ± 0.46	40.22 ± 1.21	5.15 ± 3.28

optical microscopy. The carbon electrode prepared using vacuum drying exhibits a bumpy surface, indicating that rapid solvent removal leads to bubble formation, thereby affecting the electrode morphology. In contrast, a controlled heating process allows for slower solvent evaporation, resulting in a smooth surface of carbon electrode. The current density–voltage ($J-V$) curves and PCE distribution of LTC-PSCs are shown in Figure 1a,b, and Table S1. The LTC-PSC with heating drying showed an open-circuit voltage (V_{oc}) of 0.91 V, a short-circuit current density (J_{sc}) of 19.04 mA/cm^2, and a fill factor (FF) of 55.13%, resulting in an average PCE of 9.53%, with the highest PCE being 10.10%. For the LTC-PSC prepared using vacuum drying, an average PCE of 8.39% was obtained, accompanied by a V_{oc} of 0.88 V, a J_{sc} of 17.53 mA/cm^2, and an FF of 54.64%, with the highest PCE being 8.88%. The PCE of devices prepared by using vacuum drying was 13% lower than that of heating drying. To further evaluate the effect of the drying process on the carbon electrode, the electrical properties of the carbon electrode are presented in Table S2. The carbon electrode prepared using heating drying shows higher mobility and lower sheet resistance than that prepared using vacuum drying, corresponding to the device's performance. This indicates that the quality of the carbon electrode when heating and drying is better than that when vacuum drying. Based on the drying process results, the selection of HTLs is the next phase.

The commonly used polymer donor materials were adopted to serve as an HTL for two electrode PSCs. Figure 1c,d shows the PCE distributions of PSCs with the Ag electrode (Ag-PSC) and LTC-PSC, respectively. The performance of these devices is shown in Table 1. For the PSCs using Spiro-OMeTAD, the average PCE of Ag-PSC showed promising results of 17.75%. In contrast, the average PCE of LTC-PSC using Spiro-OMeTAD was reduced to 5.15%, retaining only 29% of the

https://doi.org/10.1021/acs.energyfuels.4c03898
Energy Fuels XXXX, XXX, XXX−XXX

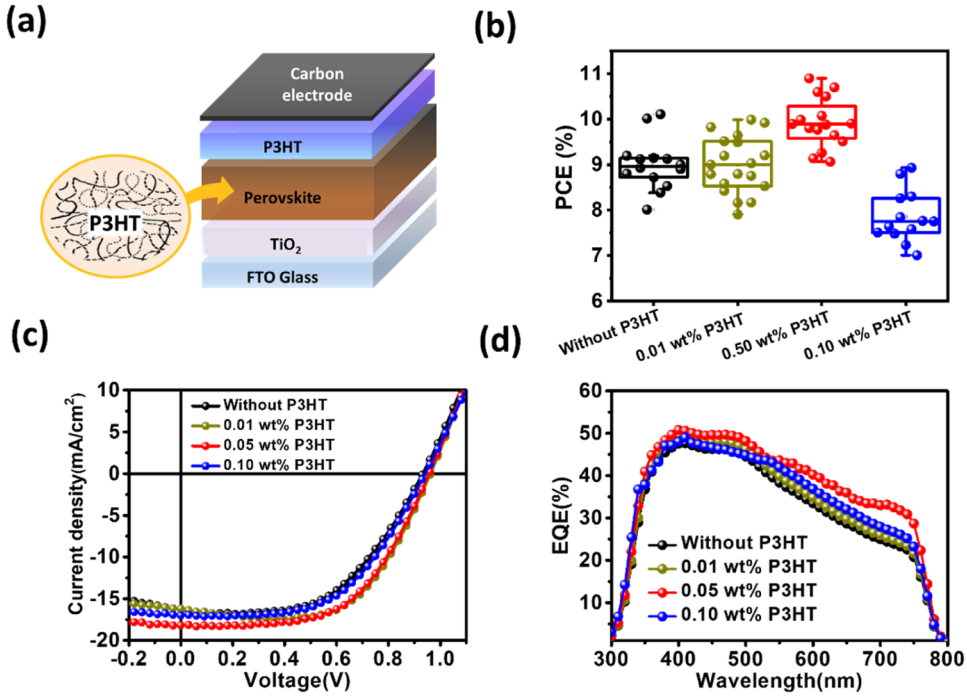

Figure 2. (a) Schematic diagram of the device structure. PSCs were prepared using perovskite films with varying concentrations of P3HT in CB: (b) PCE distributions, (c) $J-V$ curves, and (d) EQE.

Table 2. Device Performance of LTC-PSCs Prepared Using Varying Concentrations of P3HT in CB

P3HT in CB (wt %)	V_{oc} (V)	J_{sc} (mA/cm^2)	FF (%)	PCE$_{avg}$ (%)	PCE$_{champion}$ (%)
without	0.91 ± 0.03	17.93 ± 3.11	55.26 ± 2.16	9.05 ± 1.70	**10.01**
0.01	0.94 ± 0.01	16.16 ± 0.24	59.72 ± 3.75	9.09 ± 0.77	**9.90**
0.05	0.94 ± 0.02	18.53 ± 0.92	57.82 ± 0.95	10.07 ± 0.66	**10.87**
0.10	0.93 ± 0.03	17.02 ± 0.06	53.03 ± 3.22	8.39 ± 0.77	**8.93**

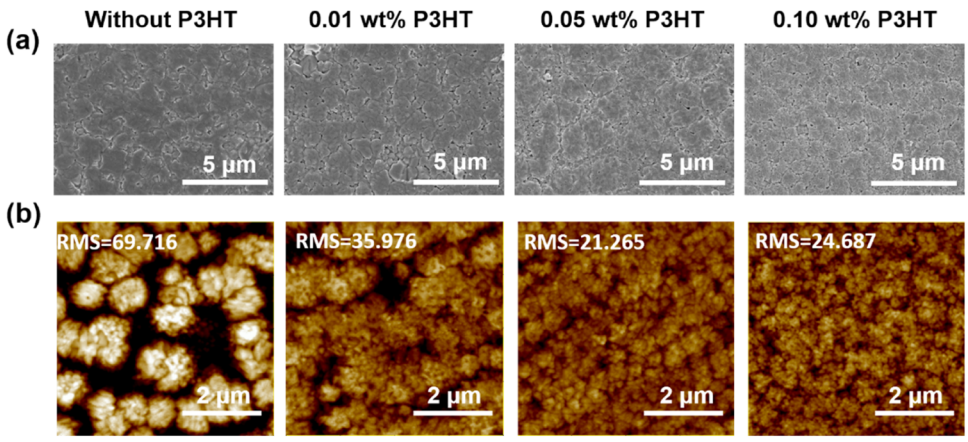

Figure 3. Morphological characteristics of perovskite films prepared using varying concentrations of P3HT in CB: (a) SEM images and (b) AFM images.

Ag-PSC performance. It indicated that the contact between Spiro-OMeTAD and the screen-printed carbon electrode resulted in significant electrical loss, making it unsuitable as the HTL for LTC-PSC. We attribute this to the manufacturing process of the carbon electrode, which involves a polar solvent, dibasic ester. This solvent may dissolve the doping salt in Spiro-OMeTAD, resulting in reduced hole mobility within the layer.[34] This finding highlights the need to identify an undoped HTL for LTC-PSCs. As shown in the energy diagram of all HTLs (Figure S2), P3HT exhibits a LUMO level comparable to that of Spiro-OMeTAD, indicating a strong potential as an ideal electron-blocking HTL. Among the other HTLs, P3HT has a high potential for use as an HTL. The average PCE of Ag-PSC using P3HT was 10.23%. Compared to that of LTC-PSC, the average PCE was slightly reduced to 9.54%, demonstrating the high potential to replace Spiro-OMeTAD for C-PSC. Therefore, P3HT was selected as the HTL of LTC-PSC for further investigation.

https://doi.org/10.1021/acs.energyfuels.4c03898
Energy Fuels XXXX, XXX, XXX−XXX

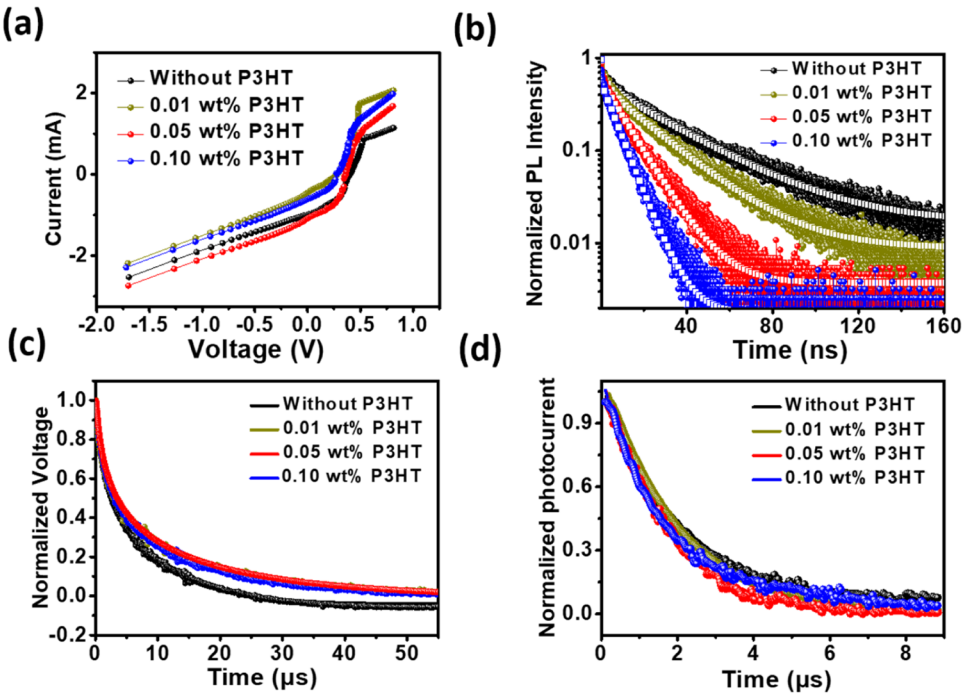

Figure 4. Electrical characteristics of the perovskite films and PSCs prepared using varying concentrations of P3HT in CB: (a) SCLC measurement of the hole-limited PSCs, (b) TRPL spectra of the perovskite films, (c) TPV spectra of LTC-PSCs, (d) TPC spectra of LTC-PSCs.

3.2. Perovskite Film Prepared Using Polymer Additive Dissolved in Antisolvent. The defect density of the perovskite film is determined by the quality of the film, which is related to the performance of the PSCs. The device structure of LTC-PSCs was FTO/TiO_2/perovskite/P3HT/C, as shown in Figure 2a. Additive engineering in the perovskite precursor solution and antisolvent dripping are widely used to improve the quality of perovskite films. In our previous studies,[28,29] the PEG polymer additive was utilized to serve as a nucleation site during perovskite formation. Considering the electronic properties of the polymer additive, the conducting polymer P3HT was carefully selected to introduce into the antisolvent chlorobenzene (CB). This addition enhances heterogeneous nucleation during film formation, promoting crystal growth rather than simply supporting nucleation. Figure 2b,c shows the PCE distributions and $J-V$ curves of LTC-PSCs prepared using different P3HT concentrations in CB. The performance of these devices is shown in Table 2. For the pristine LTC-PSC, the average PCE was 9.05%, with V_{oc}, J_{sc}, and FF values of 0.91 V, 17.93 mA/cm^2, and 55.26%, respectively. With 0.05 wt % P3HT additive in the antisolvent, the average PCE of LTC-PSCs increased to 10.07% due to the enhancement of V_{oc} and J_{sc}. The J_{sc} increased from 17.93 to 18.53 mA/cm^2, which corresponds to the improvement in the EQE measurement of Figure 2d and Table S3. When the concentration of P3HT increased to 0.10 wt % in the antisolvent, the average PCE of LTC-PSCs was reduced to 8.39% with a decrease in J_{SC} and FF. Finally, the highest PCE of the champion device reached 10.87% from the PSC prepared using 0.05 wt % P3HT dissolved in antisolvent CB. To elucidate the role of P3HT in perovskite, the morphology and electrical properties of perovskite films were further investigated.

The morphology of perovskite films was analyzed using top-view SEM images and AFM images (Figure 3). The perovskite films were deposited on the TiO_2/FTO substrate to ensure identical conditions for the devices. With 0.01 wt % P3HT in the antisolvent CB, the perovskite film showed a crystal domain size similar to the pristine perovskite film, but with some pinholes. When the P3HT concentration increased to 0.05 and 0.10 wt %, the perovskite film exhibited fewer pinholes and larger crystal domains compared to the pristine film. In AFM images, the roughness of the perovskite film was reduced from 69.7 to 36.0 nm by introducing 0.01 wt % P3HT in the antisolvent. The roughness of the perovskite film prepared using 0.05 wt % P3HT was 21.3 nm, making it the smoothest film under other concentrations. The P3HT polymer is expected to act as a trigger for heterogeneous nucleation centers during film formation, leading to rapid crystal growth and improved coverage of the perovskite film. The incorporation of P3HT in the perovskite film led to a reduction of grain boundaries, which also smoothed the roughness of the film surface.

To further understand the enhanced performance with P3HT doping, the carrier behaviors of perovskite films and devices were studied. The space-charge limited current (SCLC) curves are shown in Figure 4a. The trap density of the perovskite film can be calculated using the trap-filled-limit (TFL) equation, and the voltage at which all traps are filled is known as the trap-filled limit voltage (V_{TFL}). For a V_{TFL} measurement, the device structure adopted is FTO/TiO_2/Perovskite/PCBM/Ag. V_{TFL} was determined by fitting the slopes of the SCLC curve with the V_{TFL} equation in the trap-filled limit regime.[29,35] The calculated V_{TFL} and trap density are listed in Table S4. The trap densities of perovskite films with 0.01, 0.05, and 0.10 wt % P3HT in CB were 8.22, 7.51, and 5.87 × 10^{15} cm^{-3}, respectively, compared to the pristine perovskite film at 9.61 × 10^{15} cm^{-3}. The reduced trap density of the perovskite films corresponds to fewer grain boundaries in the perovskite film, as observed in the SEM images. In Figure 4b, the TRPL decay behavior of perovskite films was investigated. The perovskite films were prepared on the TiO_2

https://doi.org/10.1021/acs.energyfuels.4c03898
Energy Fuels XXXX, XXX, XXX−XXX

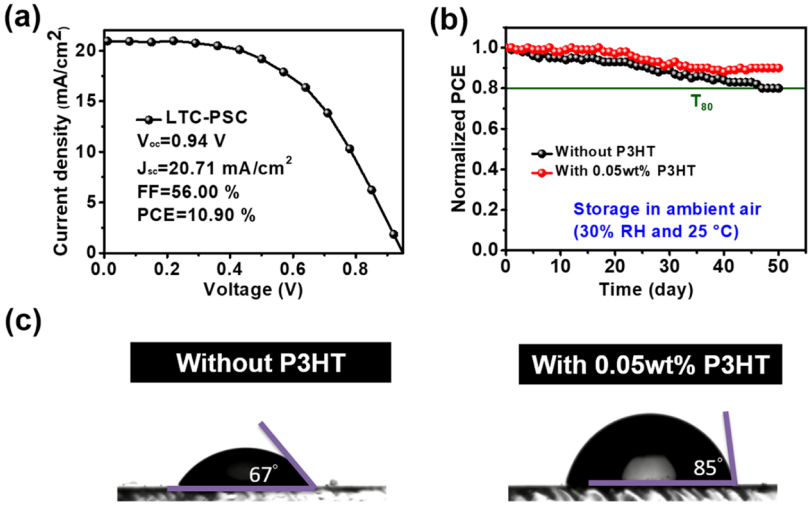

Figure 5. (a) $J-V$ curve of the champion LTC-PSC. (b) Stability of unencapsulated LTC-PSCs with and without P3HT. (c) Contact angles of the perovskite films with and without P3HT.

using different concentrations of P3HT in antisolvent CB. All of the curves are fitted with a second-order exponential decay.[36] The fitting results are listed in Table S5. The fast decay component (τ_1) is attributed to quenching trap states or interfacial charge transfer, while the slow decay component (τ_2) is attributed to bimolecular recombination via light emission.[37] The average lifetime (τ_{avg}) represents the combination of these two components. The τ_{avg} value of the pristine perovskite film was 15.11 ns. Using P3HT-containing antisolvent, the τ_{avg} of perovskite films was shortened to 12.12, 4.34, and 4.29 ns for P3HT concentrations of 0.01, 0.05, and 0.10 wt %, respectively. The shorter lifetime of the perovskite film on ETL represents that the P3HT conducting polymer in the perovskite film can facilitate charge transport. TPV and TPC measurements were used to assess carrier lifetime and extraction lifetime in the LTC-PSCs to gain insight into the whole device. The results are shown in Figure 4c,d, and the results are listed in Table S6. In TPV measurements, the carrier lifetime of LTC-PSCs prepared using the pristine perovskite film was 4.69 μs. For the perovskite film prepared using 0.01, 0.05, and 0.10 wt % P3HT in CB, the carrier lifetimes of LTC-PSCs were 4.91, 5.62, and 5.16 μs, respectively. The longest lifetime can be observed in the LTC-PSC using 0.05 wt %, which means less carrier recombination in the device. In TPC results, the carrier extraction lifetimes for LTC-PSCs using pristine, 0.01, 0.05, and 0.10 wt % were 2.08, 1.99, 1.65, and 1.78 μs, respectively. The LTC-PSC using 0.05 wt % showed the lowest carrier extraction lifetime, attributed to the P3HT in perovskite films, corresponding to the device performance. Thus, the optimal concentration of P3HT in antisolvent for the preparation of the perovskite film was determined to be 0.05 wt %. This observation suggests that while the quality of the perovskite film benefits from high P3HT content, but the charge transport properties are more favorable with 0.05 wt % P3HT than with 0.1 wt %.

To analyze the charge transport properties of LTC-PSCs, electrochemical impedance spectroscopy (EIS) has been performed, with the results presented in Figure S3 and Table S7 for devices prepared using varying concentrations of P3HT in CB. The results indicate that PSCs with 0.05 wt % P3HT exhibit a reduced charge transfer resistance (R_{ct}) compared to PSCs without P3HT, suggesting enhanced charge transfer to the adjacent layer with P3HT incorporation. However, when the P3HT concentration increases to 0.1 wt %, the R_{ct} of PSC slightly increases, consistent with the shift in the work function of the perovskite layer at this concentration. Further, the energy levels of perovskite layers, shown in Figure S4, was conducted using ultraviolet photoelectron spectroscopy (UPS). The work function of the perovskite film increases with a P3HT concentration up to 0.05 wt %, suggesting improved charge extraction in the perovskite films.[38] However, at a P3HT concentration of 0.1 wt %, the work function slightly decreases, leading to reduced charge extraction compared to the P3HT concentration of 0.05 wt %. Finally, optimized LTC-PSC was obtained. The $J-V$ curve of the champion cell, with a V_{oc} of 0.94 V, a J_{sc} of 20.71 mA/cm^2, an FF of 56%, and a PCE of 10.90%, is shown in Figure 5a. Furthermore, the stability of LTC-PSC is demonstrated in Figure 5b. The unencapsulated devices were stored in ambient air (30% relative humidity and 25 °C). After 50 days (1200 h), the LTC-PSC with 0.05 wt % P3HT maintained 90% of its initial PCE. The LTC-PSC without P3HT reduced to 80% of its initial PCE. This indicates that the perovskite film's quality is critical to LTC-PSC's long-term stability. The contact angle images of the perovskite films are illustrated in Figure 5c. The angles of the perovskite films with and without P3HT were 67 and 85°, respectively. The introduction of P3HT to the perovskite film not only improved the quality of the perovskite but also modified the perovskite surface to become hydrophobic, which helps hinder moisture penetration.

4. CONCLUSIONS

The development and characterization of low-temperature carbon electrodes were conducted by electrical measurements. Additionally, the selection of HTL and polymer additive strategies were employed. P3HT in antisolvent CB served as a nucleation site during perovskite formation, resulting in a lower defect density of the perovskite film and a homogeneous interface between the perovskite and the carbon electrode. The highest PCE achieved for LTC-PSCs was 10.90%, representing an 11% average PCE improvement compared with pristine conditions. The stability of unencapsulated LTC-PSCs retained 90% of the initial PCE after 1200 h in ambient air. These results offer a practical approach for improving the

https://doi.org/10.1021/acs.energyfuels.4c03898
Energy Fuels XXXX, XXX, XXX−XXX

quality of perovskite films and addressing interface issues in carbon-based PSCs, while also advancing low-cost electrode techniques for perovskite solar cells.

■ ASSOCIATED CONTENT

Supporting Information

The Supporting Information is available free of charge at https://pubs.acs.org/doi/10.1021/acs.energyfuels.4c03898.

Electrical characterizations of LTC electrode; performance; and SCLC, TRPL, TPC, and TPV of LTC-PSCs (PDF)

■ AUTHOR INFORMATION

Corresponding Authors

Ming-Chung Wu − *Center for Sustainability and Energy Technologies, Chang Gung University, Taoyuan 333323, Taiwan; Department of Chemical and Materials Engineering, Chang Gung University, Taoyuan 333323, Taiwan; Division of Neonatology, Department of Pediatrics, Chang Gung Memorial Hospital at Linkou, Taoyuan 333423, Taiwan; Department of Materials Engineering, Ming Chi University of Technology, New Taipei 243303, Taiwan;* orcid.org/0000-0002-3584-3871; Email: mingchungwu@mail.cgu.edu.tw

Yu-Ching Huang − *Center for Sustainability and Energy Technologies, Chang Gung University, Taoyuan 333323, Taiwan; Organic Electronics Research Center, Ming Chi University of Technology, New Taipei 243303, Taiwan; Department of Chemical and Materials Engineering, Chang Gung University, Taoyuan 333323, Taiwan; Department of Materials Engineering, Ming Chi University of Technology, New Taipei 243303, Taiwan;* orcid.org/0000-0003-4772-8050; Email: huangyc@mail.mcut.edu.tw

Authors

Shih-Han Huang − *Center for Sustainability and Energy Technologies, Chang Gung University, Taoyuan 333323, Taiwan; Organic Electronics Research Center, Ming Chi University of Technology, New Taipei 243303, Taiwan;* orcid.org/0009-0002-8344-4645

Yu-Hsiang Chen − *Department of Chemical and Materials Engineering, Chang Gung University, Taoyuan 333323, Taiwan*

Hou-Chin Cha − *Organic Electronics Research Center, Ming Chi University of Technology, New Taipei 243303, Taiwan*

Damian Glowienka − *Faculty of Applied Physics and Mathematics, Gdańsk University of Technology, Gdańsk 80-233, Poland;* orcid.org/0000-0001-5508-2929

Complete contact information is available at: https://pubs.acs.org/10.1021/acs.energyfuels.4c03898

Notes

The authors declare no competing financial interest.

■ ACKNOWLEDGMENTS

Financial support provided by the National Science and Technology Council of Taiwan (Grant Nos. NSTC 112-2628-E-131-001-MY4, NSTC 113-2628-E-182-001-MY4, NSCT 111-2221-E-182-040-MY3, NSTC 112-2622-E-131-001, NSTC 113-2622-E-131-006-, NSTC 111-2923-E-002-012-MY3, NSTC 111-2923-E-002-007-MY3, and NSTC 113-2221-E-003-001) is highly appreciated. The authors thank the support from Chang Gung University (URRPD2N0011 and URRPD2N0031) and Chang Gung Memorial Hospital at Linkou (CMRPD2N0061 and BMRPC74), which is highly appreciated. This research was partly funded by the National Science Centre, in cooperation with the M-ERA.NET 3 Call 2021 for grant no. 2021/03/Y/ST5/00233. This project received funding from the European Union's Horizon 2020 research and innovation program under grant agreement no. 958174.

■ REFERENCES

(1) Kojima, A.; Teshima, K.; Shirai, Y.; Miyasaka, T. Organometal Halide Perovskites as Visible-Light Sensitizers for Photovoltaic Cells. *J. Am. Chem. Soc.* **2009**, *131* (17), 6050−6051.

(2) Huang, Z.; Bai, Y.; Huang, X.; Li, J.; Wu, Y.; Chen, Y.; Li, K.; Niu, X.; Li, N.; Liu, G.; et al. Anion−π interactions suppress phase impurities in FAPbI3 solar cells. *Nature* **2023**, *623* (7987), 531−537.

(3) Qiao, J. Editorial for the special issue "CO2 Reductions to Fuels and Carbon Feedstocks. *Mater. Rep.: Energy* **2023**, *3* (2), No. 100202.

(4) Song, T.-B.; Chen, Q.; Zhou, H.; Jiang, C.; Wang, H.-H.; Yang, Y.; Liu, Y.; You, J.; Yang, Y. Perovskite solar cells: film formation and properties. *J. Mater. Chem. A* **2015**, *3* (17), 9032−9050.

(5) Yue, Y.; Salim, N.; Wu, Y.; Yang, X.; Islam, A.; Chen, W.; Liu, J.; Bi, E.; Xie, F.; Cai, M.; Han, L. Enhanced Stability of Perovskite Solar Cells through Corrosion-Free Pyridine Derivatives in Hole-Transporting Materials. *Adv. Mater.* **2016**, *28* (48), 10738−10743.

(6) Wu, T.; Zhuang, R.; Zhao, R.; Zhao, R.; Zhu, L.; Liu, G.; Wang, R.; Zhao, K.; Hua, Y. Understanding the Effects of Fluorine Substitution in Lithium Salt on Photovoltaic Properties and Stability of Perovskite Solar Cells. *ACS Energy Lett.* **2021**, *6* (6), 2218−2228.

(7) Meng, D.; Xue, J.; Zhao, Y.; Zhang, E.; Zheng, R.; Yang, Y. Configurable Organic Charge Carriers toward Stable Perovskite Photovoltaics. *Chem. Rev.* **2022**, *122* (18), 14954−14986.

(8) Domanski, K.; Correa-Baena, J.-P.; Mine, N.; Nazeeruddin, M. K.; Abate, A.; Saliba, M.; Tress, W.; Hagfeldt, A.; Grätzel, M. Not All That Glitters Is Gold: Metal-Migration-Induced Degradation in Perovskite Solar Cells. *ACS Nano* **2016**, *10* (6), 6306−6314.

(9) Meroni, S. M. P.; Hooper, K. E. A.; Dunlop, T.; Baker, J. A.; Worsley, D.; Charbonneau, C.; Watson, T. M. Scribing Method for Carbon Perovskite Solar Modules. *Energies* **2020**, *13* (7), No. 1589.

(10) Bogachuk, D.; Zouhair, S.; Wojciechowski, K.; Yang, B.; Babu, V.; Wagner, L.; Xu, B.; Lim, J.; Mastroianni, S.; Pettersson, H.; et al. Low-temperature carbon-based electrodes in perovskite solar cells. *Energy Environ. Sci.* **2020**, *13* (11), 3880−3916.

(11) Chen, J.; Xiong, Y.; Rong, Y.; Mei, A.; Sheng, Y.; Jiang, P.; Hu, Y.; Li, X.; Han, H. Solvent effect on the hole-conductor-free fully printable perovskite solar cells. *Nano Energy* **2016**, *27*, 130−137.

(12) Zhou, H.; Shi, Y.; Dong, Q.; Zhang, H.; Xing, Y.; Wang, K.; Du, Y.; Ma, T. Hole-Conductor-Free, Metal-Electrode-Free TiO2/CH3NH3PbI3 Heterojunction Solar Cells Based on a Low-Temperature Carbon Electrode. *J. Phys. Chem. Lett.* **2014**, *5* (18), 3241−3246.

(13) Ku, Z.; Rong, Y.; Xu, M.; Liu, T.; Han, H. Full Printable Processed Mesoscopic CH3NH3PbI3/TiO2 Heterojunction Solar Cells with Carbon Counter Electrode. *Sci. Rep.* **2013**, *3* (1), No. 3132.

(14) Hu, Y.; Si, S.; Mei, A.; Rong, Y.; Liu, H.; Li, X.; Han, H. Stable Large-Area (10 × 10 cm^2) Printable Mesoscopic Perovskite Module Exceeding 10% Efficiency. *Sol. RRL* **2017**, *1* (2), No. 1600019.

(15) Mei, A.; Li, X.; Liu, L.; Ku, Z.; Liu, T.; Rong, Y.; Xu, M.; Hu, M.; Chen, J.; Yang, Y.; et al. A hole-conductor−free, fully printable mesoscopic perovskite solar cell with high stability. *Science* **2014**, *345* (6194), 295−298.

(16) Jiang, S.; Sheng, Y.; Hu, Y.; Rong, Y.; Mei, A.; Han, H. Influence of precursor concentration on printable mesoscopic perovskite solar cells. *Front. Optoelectron.* **2020**, *13* (3), 256−264.

(17) Liu, S.; Huang, W.; Liao, P.; Pootrakulchote, N.; Li, H.; Lu, J.; Li, J.; Huang, F.; Shai, X.; Zhao, X.; et al. 17% efficient printable mesoscopic PIN metal oxide framework perovskite solar cells using

cesium-containing triple cation perovskite. *J. Mater. Chem. A* **2017**, *5* (44), 22952−22958.
(18) Chu, Q.-Q.; Ding, B.; Peng, J.; Shen, H.; Li, X.; Liu, Y.; Li, C.-X.; Li, C.-J.; Yang, G.-J.; White, T. P.; Catchpole, K. R. Highly stable carbon-based perovskite solar cell with a record efficiency of over 18% via hole transport engineering. *J. Mater. Sci. Technol.* **2019**, *35* (6), 987−993.
(19) Babu, V.; Pineda, R. F.; Ahmad, T.; Alvarez, A. O.; Castriotta, L. A.; Di Carlo, A.; Fabregat-Santiago, F.; Wojciechowski, K. Improved Stability of Inverted and Flexible Perovskite Solar Cells with Carbon Electrode. *ACS Appl. Energy Mater.* **2020**, *3* (6), 5126−5134.
(20) Zouhair, S.; Yoo, S.-M.; Bogachuk, D.; Herterich, J. P.; Lim, J.; Kanda, H.; Son, B.; Yun, H. J.; Würfel, U.; Chahboun, A.; et al. Employing 2D-Perovskite as an Electron Blocking Layer in Highly Efficient (18.5%) Perovskite Solar Cells with Printable Low Temperature Carbon Electrode. *Adv. Energy Mater.* **2022**, *12* (21), No. 2200837.
(21) Du, T.; Qiu, S.; Zhou, X.; Le Corre, V. M.; Wu, M.; Dong, L.; Peng, Z.; Zhao, Y.; Jang, D.; Spiecker, E.; et al. Efficient, stable, and fully printed carbon-electrode perovskite solar cells enabled by hole-transporting bilayers. *Joule* **2023**, *7* (8), 1920−1937.
(22) Xiao, Z.; Dong, Q.; Bi, C.; Shao, Y.; Yuan, Y.; Huang, J. Solvent Annealing of Perovskite-Induced Crystal Growth for Photovoltaic-Device Efficiency Enhancement. *Adv. Mater.* **2014**, *26* (37), 6503−6509.
(23) Aydin, E.; De Bastiani, M.; De Wolf, S. Defect and Contact Passivation for Perovskite Solar Cells. *Adv. Mater.* **2019**, *31* (25), No. 1900428.
(24) Gao, D.; Li, B.; Li, Z.; Wu, X.; Zhang, S.; Zhao, D.; Jiang, X.; Zhang, C.; Wang, Y.; Li, Z.; et al. Highly Efficient Flexible Perovskite Solar Cells through Pentylammonium Acetate Modification with Certified Efficiency of 23.35%. *Adv. Mater.* **2023**, *35* (3), No. 2206387.
(25) Mann, D. S.; Patil, P.; Kwon, S.-N.; Na, S.-I. Enhanced performance of p-i-n perovskite solar cell via defect passivation of nickel oxide/perovskite interface with self-assembled monolayer. *Appl. Surf. Sci.* **2021**, *560*, No. 149973.
(26) Jin, L.; Liu, X.; Li, Y.-L.; Zhou, J.; Fu, W. 4-biphenylcarboxylic acid as defect passivation for high-efficient perovskite solar cells. *Appl. Surf. Sci.* **2023**, *635*, No. 157733.
(27) Shen, W.; Dong, Y.; Huang, F.; Cheng, Y.-B.; Zhong, J. Interface passivation engineering for hybrid perovskite solar cells. *Mater. Rep.: Energy* **2021**, *1* (4), No. 100060.
(28) Chang, C.-Y.; Chu, C.-Y.; Huang, Y.-C.; Huang, C.-W.; Chang, S.-Y.; Chen, C.-A.; Chao, C.-Y.; Su, W.-F. Tuning Perovskite Morphology by Polymer Additive for High Efficiency Solar Cell. *ACS Appl. Mater. Interfaces* **2015**, *7* (8), 4955−4961.
(29) Huang, S.-H.; Tian, K.-Y.; Huang, H.-C.; Li, C.-F.; Chu, W.-C.; Lee, K.-M.; Huang, Y.-C.; Su, W.-F. Controlling the Morphology and Interface of the Perovskite Layer for Scalable High-Efficiency Solar Cells Fabricated Using Green Solvents and Blade Coating in an Ambient Environment. *ACS Appl. Mater. Interfaces* **2020**, *12* (23), 26041−26049.
(30) Huang, S.-H.; Guan, C.-K.; Lee, P.-H.; Huang, H.-C.; Li, C.-F.; Huang, Y.-C.; Su, W.-F. Toward All Slot-Die Fabricated High Efficiency Large Area Perovskite Solar Cell Using Rapid Near Infrared Heating in Ambient Air. *Adv. Energy Mater.* **2020**, *10* (37), No. 2001567.
(31) Bi, D.; Yi, C.; Luo, J.; Décoppet, J.-D.; Zhang, F.; Zakeeruddin, S. M.; Li, X.; Hagfeldt, A.; Grätzel, M. Polymer-templated nucleation and crystal growth of perovskite films for solar cells with efficiency greater than 21%. *Nat. Energy* **2016**, *1*, No. 16142.
(32) Qin, P.-L.; Yang, G.; Ren, Z.-W.; Cheung, S. H.; So, S. K.; Chen, L.; Hao, J.; Hou, J.; Li, G. Stable and Efficient Organo-Metal Halide Hybrid Perovskite Solar Cells via π-Conjugated Lewis Base Polymer Induced Trap Passivation and Charge Extraction. *Adv. Mater.* **2018**, *30* (12), No. 1706126.
(33) Chen, S.-H.; Chan, S.-H.; Lin, Y.-T.; Wu, M.-C. Enhanced power conversion efficiency of perovskite solar cells based on mesoscopic Ag-doped TiO2 electron transport layer. *Appl. Surf. Sci.* **2019**, *469*, 18−26.
(34) Li, Y.; Li, H.; Zhong, C.; Sini, G.; Brédas, J.-L. Characterization of intrinsic hole transport in single-crystal spiro-OMeTAD. *npj Flexible Electron.* **2017**, *1* (1), No. 2.
(35) Huang, S.-H.; Wang, Y.-C.; Hsiao, K.-C.; Lee, P.-H.; Liao, H.-C.; Huang, Y.-X.; Huang, Y.-C.; Su, W.-F. Solid-State Ligand-Capped Metal Oxide Electron-Transporting Layer for Efficient and Stable Fullerene-Free Perovskite Solar Cells. *Sol. RRL* **2022**, *6* (2), No. 2100671.
(36) Chen, Q.; Zhou, H.; Song, T.-B.; Luo, S.; Hong, Z.; Duan, H.-S.; Dou, L.; Liu, Y.; Yang, Y. Controllable Self-Induced Passivation of Hybrid Lead Iodide Perovskites toward High Performance Solar Cells. *Nano Lett.* **2014**, *14* (7), 4158−4163.
(37) Zuo, L.; Chen, Q.; De Marco, N.; Hsieh, Y.-T.; Chen, H.; Sun, P.; Chang, S.-Y.; Zhao, H.; Dong, S.; Yang, Y. Tailoring the Interfacial Chemical Interaction for High-Efficiency Perovskite Solar Cells. *Nano Lett.* **2017**, *17* (1), 269−275.
(38) Cheng, J.; Xie, F.; Liu, Y.; Sha, W. E. I.; Li, X.; Yang, Y.; Choy, W. C. H. Efficient hole transport layers with widely tunable work function for deep HOMO level organic solar cells. *J. Mater. Chem. A* **2015**, *3* (47), 23955−23963.

https://doi.org/10.1021/acs.energyfuels.4c03898
Energy Fuels XXXX, XXX, XXX−XXX